Journal of Applied Physics

RESEARCH ARTICLE | SEPTEMBER 11 2018

Flash-sintering of antimony telluride and its thermoelectric properties

Masashi Mikami ; Yoshiaki Kinemuchi; Kazuya Kubo; Naoki Uchiyama; Hidetoshi Miyazaki; Yoichi Nishino

Check for updates

J. Appl. Phys. 124, 105104 (2018)
https://doi.org/10.1063/1.5041970

View Online Export Citation

Articles You May Be Interested In

Transport properties of electrically sintered bismuth antimony telluride with antimony nanoprecipitation
Appl. Phys. Lett. (October 2017)

Studies on antimony telluride thin films as buffer layer for solar cell applications
J. Renewable Sustainable Energy (June 2013)

High Seebeck coefficient in thermally evaporated Sb-In co-alloyed bismuth telluride thin film
J. Appl. Phys. (February 2020)

09 July 2025 02:46:38

Journal of Applied Physics
Special Topics
Open for Submissions
Learn More
AIP Publishing

AIP Publishing

Flash-sintering of antimony telluride and its thermoelectric properties

Masashi Mikami,[1] Yoshiaki Kinemuchi,[1] Kazuya Kubo,[2] Naoki Uchiyama,[2]
Hidetoshi Miyazaki,[3] and Yoichi Nishino[3]
[1]*National Institute of Advanced Industrial Science and Technology, Nagoya 463-8560, Japan*
[2]*Atsumitec Co., Ltd., Hamamatsu 431-0192, Japan*
[3]*Nagoya Institute of Technology, Nagoya 466-8555, Japan*

(Received 28 May 2018; accepted 23 August 2018; published online 11 September 2018)

This study set out to examine the flash sintering of thermoelectric materials. A finite element method analysis of electric current activated/assisted sintering with an insulating mold suggested that the use of a sufficiently high Joule-heating rate, such as >10 000 K/s, relative to the thermal diffusion rate of the mold material, can realize uniform sample heating. Based on the analysis results, the sintering of Sb_2Te_3, a typical thermoelectric material, was conducted with a current feed duration of 1 s, using a sintering apparatus that had been specially devised for flash-sintering. Although a slight reduction in the density and degree of grain alignment was observed, the crystallographic phase was unaffected by the rapid heating, with the thermoelectric performance of the Sb_2Te_3 sample prepared by the 1-s sintering being comparable with that of a sample that had been conventionally sintered at 773 K for 3 min. This significant reduction in the sintering time can result in the energy consumption for the sintering process being decreased to less than 1% of that required for conventional current sintering. This significant energy-conservation effect of the flash sintering should be appealing from a practical point of view, especially for the fabrication of those thermoelectric materials used for power generation and aimed at energy recovery. *Published by AIP Publishing.* https://doi.org/10.1063/1.5041970

I. INTRODUCTION

Thermoelectric (TE) conversion technology has recently attracted renewed interest given the potential for its application to the effective utilization of energy resources. In particular, energy recovery from currently wasted heat is an obvious target for TE power generation because TE conversion systems are highly adaptable to a wide range of heat sources, temperatures, and energy scales, including industrial waste heat, vehicle exhausts, and even human body heat. The conversion efficiency of TE devices depends mainly on the performance of the TE materials, which is evaluated using a so-called "thermoelectric figure of merit," $ZT = (S^2\sigma/\kappa)T$, where S is the Seebeck coefficient, σ is the electrical conductivity, κ is the thermal conductivity, and T is the absolute temperature. Therefore, high-performance TE materials having a particular combination of transport properties, specifically, a large S, high σ, and low κ, are required. However, materials possessing a high Z value as an intrinsic property are rare because the demands made of TE materials conflict with one another in terms of carrier density, electronic structure, and crystalline nature.[1] Microstructure refinement is therefore an effective means of improving the TE performance when the electronic and thermal properties are independently controlled by artificially introduced microstructures such as grain boundaries, interfaces, and defects.[2–4]

A powder metallurgical technique is commonly used for the fabrication of a fine-grain sintered body. In particular, electric current activated/assisted sintering [ECAS, also known as spark plasma sintering (SPS)] is an effective means of preparing sintered materials having a fine microstructure because of the rapid densification of the finely powdered materials with limited grain growth by abrupt heating/cooling under pressure.[5–7] In the past few decades, the efficacy of microstructure modification by ECAS with the goal of improving the TE performance has been demonstrated in a number of material studies.[8–10] In these previous studies, nanoscale texture control has been achieved using the ECAS process with the application of mechanical pressure for several minutes.

In the study of ECAS, flash sintering (FS), which is defined as sintering with a duration on the order of seconds,[11] is attracting increasing levels of attention as a result of a study in which ionic conductive zirconia was successfully sintered in a few seconds.[12] Since then, FS has been applied mainly to ceramics, utilizing a thermal runaway phenomenon that is triggered by applying a strong electrical field, and which affects the ionic and semiconducting transport properties, i.e., a steeply increasing σ with an increase in T.[13–17] Although it has been suggested that FS could potentially be used to realize the further modification of sintered materials,[10] to date there have not been enough studies of the transport properties of FS materials, especially TE materials. In the present study, as a first step toward the development of FS for TE materials, the conditions necessary to enable the sintering of TE materials within a few seconds were examined by undertaking a finite element method (FEM) analysis, after which FS equipment was specially developed based on the FEM results. In addition, a typical TE material, namely, Sb_2Te_3, was sintered with a current feed duration of 1 s, after which its TE properties were evaluated.

II. EXPERIMENTAL

To enable an estimation of the sample temperature distribution during ECAS, FEM analyses were conducted using

09 July 2025 02:46:38

the COMSOL Multiphysics software with a 2D axisymmetric geometry in a time-dependent mode. The configured sample measured Ø10 mm × 3 mm. Assuming that ECAS would be conducted in a vacuum, the boundaries of the surface were assigned thermal radiation values, except for the top/bottom surfaces of the copper electrode which had a heat transfer coefficient of 10 000 W/m^2K, assuming water cooling. The influence of the heating rate on the sample temperature distribution was examined. For simplicity, the temperature dependence of the material properties, shrinkage behavior, electrical conduction of the zirconia die including ionic conduction, and Seebeck/Peltier effects were excluded.

Based on the FEM results, a dedicated FS apparatus was fabricated. Although the main components of this FS equipment were the same as those of a conventional ECAS setup, including the electrical power source, mechanical pressure device, and vacuum chamber, the controllable time scale of the power supply was modified to be on the order of milliseconds. In addition, to cancel out the Seebeck/Peltier effect by feeding current through the TE materials, a 100-Hz alternating current with a trapezoidal waveform was used as the power source. On the other hand, a temperature-measuring system was excluded because a practical means of measuring the temperature inside the sintering mold with a time-resolution on the order of milliseconds was not available. Using the developed FS equipment, commercial Sb_2Te_3 powder (99.9%, Kojundo Chemical Lab. Co., Ltd.) was sintered in a vacuum of <10 Pa under a uniaxial pressure of 32 MPa, using a stabilized zirconia mold and graphite punch, with current being applied for 1 s. For the mold material, 3 mol. % yttria-stabilized zirconia with a high electrical resistance of $>10^{10}$ Ωm at room temperature was employed. Although the zirconia exhibits electrical conductivity with ionic conduction, especially at high temperatures, it is safe to assume that the electrical conductivity of the zirconia mold has a negligibly small influence on the temperature distribution in the sample during ECAS. This is because the σ value of the zirconia is several orders of magnitude lower than that of the graphite punch and Sb_2Te_3 at the low sintering temperature (<800 K) in a weak electrical field (less than 5 V/cm at a current feed of 1.2 kA) and with a low-frequency current (100 Hz). For comparison, a conventional ECAS machine (LABOX-625FC, Sinter Land Inc.) was used to sinter the same Sb_2Te_3 powder at 773 K for 3 min in a vacuum under a uniaxial pressure of 50 MPa, using a graphite mold and punch. In this case, the heating and cooling rates were both 100 K/min. The obtained bulk samples, with a typical size of Ø10 mm × 2 mm, were first used to acquire the value of κ and were then cut into bar shapes with a typical size of $2 \times 2 \times 9\ mm^3$ for the measurement of σ and S.

Crystalline phase analysis was performed using X-ray diffraction (XRD) with Cu Kα radiation. A microstructural observation was conducted using scanning electron microscopy (SEM). S and σ were simultaneously measured in a He atmosphere. The value of σ was determined using a conventional four-probe DC technique. Then, S was calculated from a plot of the thermoelectric voltage versus the temperature difference, while κ was evaluated from the density (D), thermal diffusivity (α), and specific heat (C_p), given the relationship $\kappa = D \times \alpha \times C_p$. Finally, D was calculated from the volume and weight of the specimens, and α and C_p were evaluated using the laser-flash method.

III. RESULTS AND DISCUSSION

For the sintering process, although it is apparent that the temperature and temperature uniformity within a sample are the most important parameters, mechanical pressure also plays a significant role in microstructure refinement, which is especially important for the further enhancement of TE performance because the compression of the particles is central to the densification at lower temperatures with limited grain growth. Therefore, in the present study, ECAS using a sintering mold was examined. As a first step toward the development of FS of TE materials, the relationship between the heating rate and the sample temperature distribution in the sintering mold was examined by performing a FEM analysis.

As shown in Fig. 1(a), a configuration similar to that used for conventional ECAS (with a die and a punch) was built, using the material properties listed in Table I. For the sintering sample, typical TE transport properties were applied. Note that a non-conventional insulating zirconia die was used in our model, while a conductive graphite die is usually employed for ECAS. In addition, the effects of the temperature dependence of the material properties, electrical conductivity of the zirconia die (including ionic conduction), shrinkage of the sample, and Seebeck/Peltier effect on the sintering were such that they could safely be excluded from the calculations, thus simplifying the evaluation of the relationship between the heating rate and the temperature distribution. Using this model, the current needed to heat the sample center to 1273 K in a given period, t_s, was sought and the temperature uniformity within the sample was examined.

As shown in Fig. 1(b), when t_s was on the order of minutes (say, 600 s), the high-temperature region (including the die part) was extended, resulting in a highly uniform temperature distribution within the sample. Then, if t_s was decreased, corresponding to an increase in the heating rate, the extent of the heating was reduced and the sample temperature distribution became non-uniform until $t_s \approx 1$ s. Interestingly, however, when t_s was further shortened (say, to 0.01 s), the high-temperature area was limited to the current path and the temperature uniformity within the sample was improved except at the edges. This heating rate dependence of the temperature distribution is clearly indicated in Fig. 2. This tendency can be quantitatively explained as being a result of the variation in the balance between the Joule-heating of the current path and thermal diffusion into the non-heating insulating mold. In other words, if the sample is heated to a point sufficiently higher than the thermal diffusion rate of the mold material (e.g., $1\ mm^2/s$ for zirconia), the ideal temperature uniformity can be achieved inside the sample. The results of FEM analysis were such that it was thought that the sample heating uniformity could be enhanced by increasing the heating rate to more than 10 000 K/s, for which a current of 3 kA would be necessary.

In addition, FEM analysis revealed that a conventional graphite die would be unsuitable for incorporation into our

09 July 2025 02:46:38

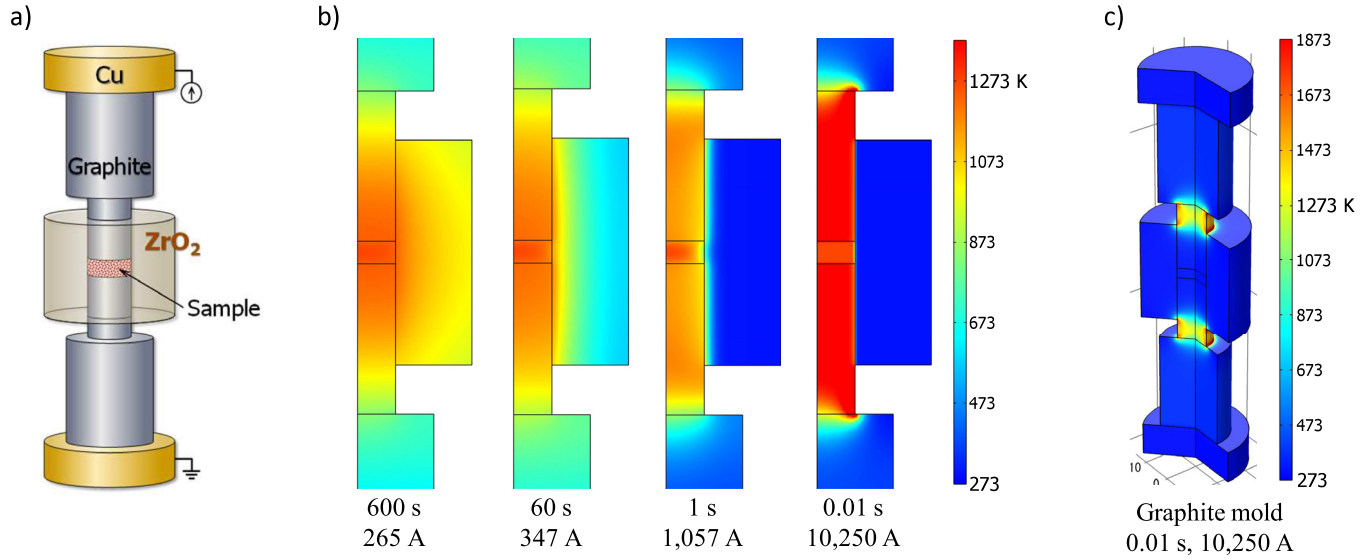

FIG. 1. (a) Configuration for FEM analysis of the ECAS-produced sample. The sample measured Ø10 mm × 3 mm thick. Joule-heating of the sample center to 1273 K over different durations was examined. (b) Images of calculated temperature distribution with different heating rates. The duration and level of feed current appears below each image. (c) 3D image of temperature distribution in a graphite mold with a current feed of 10 250 A for 0.01 s.

FS model because its use would lead to unbalanced heating resulting from the bottleneck in the current path at the punch outside the die. For instance, as shown in Fig. 1(c), if the same current feed duration as that for the zirconia die ($t_s = 0.01$) were to be applied to the graphite die model, the sample itself would be barely heated while the bottleneck with the higher electrical resistance would be heated to nearly 2000 K. Although this imbalanced heating could be partially mitigated by reducing the diameter of the graphite die, the bottleneck effect can only be reduced to a certain extent since the die must be sufficiently thick to realize a level of mechanical strength capable of withstanding mechanical pressure on the order of MPa. Another important point to note is the drastic reduction in the energy consumption of ECAS by shortening the duration. As shown in Fig. 3, the difference between the current estimated by FEM analysis (■) and the minimum value (●), as calculated from the heat capacity of the sample and the increase in the temperature, decreased as t_s became shorter. This means that the input power can be more effectively used for the heating of the sample before thermal dissipation at $t_s < 1$ s. Consequently, the energy consumption could be reduced 40-fold by shortening the current feed time from 600 s to 0.01 s. From a practical point of view, this energy-conservation effect of FS should be appealing, especially for the fabrication of the TE materials to be used for power generation aimed at energy recovery.

TABLE I. Material parameters for FEM analysis. The material properties of copper were taken from the material database incorporated into the COMSOL software. For the graphite and zirconia, the values obtained for the materials used for the FS experiment were applied. For the material properties of sample, typical values for a thermoelectric material were arbitrarily assigned.

Material	D (kg/m^3)	σ (S/m)	C_p (J/kgK)	κ (W/mK)
Copper	8700	6×10^7	385	400
Graphite	1840	7.5×10^4	1300	65
Zirconia	6000	0	600	3.2
Sample	5000	7×10^4	500	5

To practically evaluate the effect of FS on the properties of a TE material, a typical TE material, namely, Sb_2Te_3, was sintered using the equipment that had been specially designed for FS, based on the FEM results. For the first trial, when sintering was examined with a current feed duration of 0.1 s according to the FEM results, all the resulting samples had cracks along the current path. With FS, any initial small non-uniformity within the sample, such as those deriving from non-homogeneous powder compaction, seemed to cause a large non-uniformity in the heating effect. This tendency was assumed to arise as follows: (1) An initial small non-uniformity in the electrical resistance, such as that arising from non-homogeneous powder compaction, leads to an imbalance in the current density within a sample because the

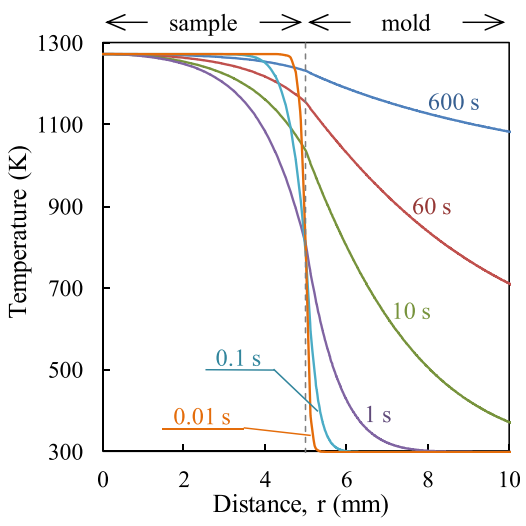

FIG. 2. Temperature calculated as part of FEM analysis along the horizontal line from the sample center to the mold, for different heating rates.

09 July 2025 02:46:38

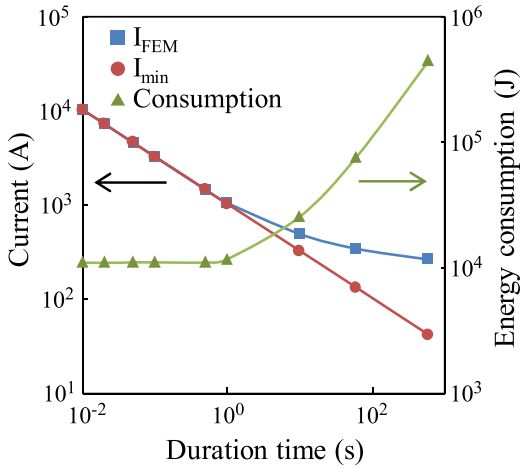

FIG. 3. Current estimated from FEM analysis (■) and minimum value (●), which was calculated from the relationship $R_{sample}I^2t_s = C_{sample}dT$ (R_{sample}: electrical resistance of sample, t_s: current feed duration, C_{sample}: heat capacity of sample, dT: rise in temperature. In this case, the assigned values were $R_{sample} = 0.55$ mΩ, $C_{sample} = 0.59$ J/K, $dT = 1000$ K). The estimated energy consumption (▲) calculated from the relationship $R_{total}I_{FEM}{}^2t_s$, where R_{total} (10.55 mΩ) was the total electrical resistance of the FEM configuration, including the copper electrode, graphite mold, and sample, while I_{FEM} was the feed current estimated by FEM analysis.

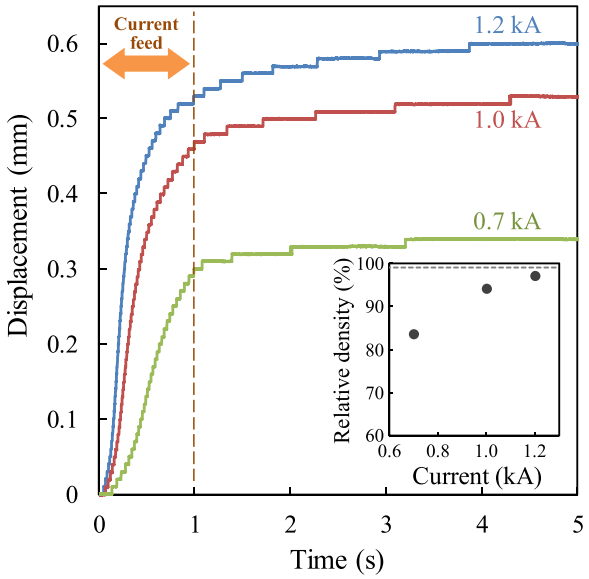

FIG. 4. Displacement of punch during Sb_2Te_3 sintering. The displacement was closely related to the shrinkage of the sample although thermal expansion/shrinkage of the electrode and punch also contributed to the displacement. The densities of the samples obtained with the different feed currents are indicated in the inset. The dotted line in the inset is the density of the Sb_2Te_3 sample prepared by the conventional ECAS process (773 K/3 min).

current flow tends to concentrate in those parts presenting a lower resistance. (2) That part of the sample with the higher current density realizes a higher sintering rate prior to other areas, due to the higher Joule-heating effect. (3) The local reduction in the electrical resistance in that part of the sample which is sintered first leads to an increase in the imbalance in the current density and the Joule-heating effect. (4) Consequently, an inhomogeneous degree of sintering within a sample could arise. In this scenario, since the chain of events is a positive feedback cycle, the initial trivial nonuniformity could result in a large degree of inhomogeneous sintering. Although this chain effect can be negated by thermal diffusion in the conventional time scale of ECAS, the rapid heating rate in FS, which is equal to or higher than the thermal diffusion, seems to make the chain effect nonnegligible.

To partially employ the thermal diffusion effect in FS, the current feed time was extended and FS with a duration of 1 s was examined. In this case, sintered samples without any cracks were obtained. As shown in Fig. 4, the rapid but smooth shrinkage curve indicated that the stable sintering behavior proceeded within some seconds. The sample density increased with the feed current, reaching a relative density of 97% at 1.2 kA. In addition, as shown in Fig. 5, a sufficiently densified and homogeneous microstructure was confirmed in almost all parts of the sample except for an outer rim around 0.3 mm from the edge. Interestingly, by comparing the original Sb_2Te_3 powder [Fig. 5(a)] and the FS sample [Fig. 5(c)], the grains appear to have grown with the evolution of the orientation texture derived from the anisotropic crystal structure of the Sb_2Te_3 within a period of seconds although the plate-like particles of Sb_2Te_3 powder align easily as a result of compaction.

The orientation texture was also confirmed by XRD, as shown in Fig. 6. As shown in Fig. 6(a), the higher 00l diffraction peaks, such as 0015 at $2\theta = 44.6$ from the sample surface perpendicular to the direction of the compression applied during sintering, indicate the preferred orientation of the 00l plane. The XRD pattern from a cross section of the sample parallel to the direction of compression supported this supposition by the higher 110 peak at $2\theta = 42.3$, as shown in Fig. 6(b). However, the lower peak intensity and the broader peak width of the 00l peak of the FS sample, relative to that for the sample sintered with the conventional ECAS process (773 K/3 min) [see Fig. 6(c)], suggested that the degree of orientation in the FS sample is slightly lower than that of the conventional ECAS sample. Actually, by using Lotgering factor F, which can be used to roughly

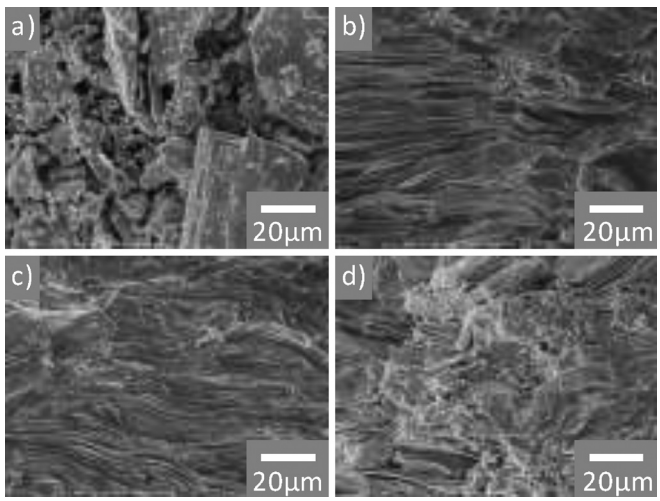

FIG. 5. SEM images of (a) original Sb_2Te_3 powder and fracture cross-sections of sintered sample prepared by (b) conventional ECAS process (773 K/3 min), and (c) and (d) current feed of 1.2 kA for 1 s. (c) and (d) were taken from the center of the sample and at the edge, respectively.

09 July 2025 02:46:38

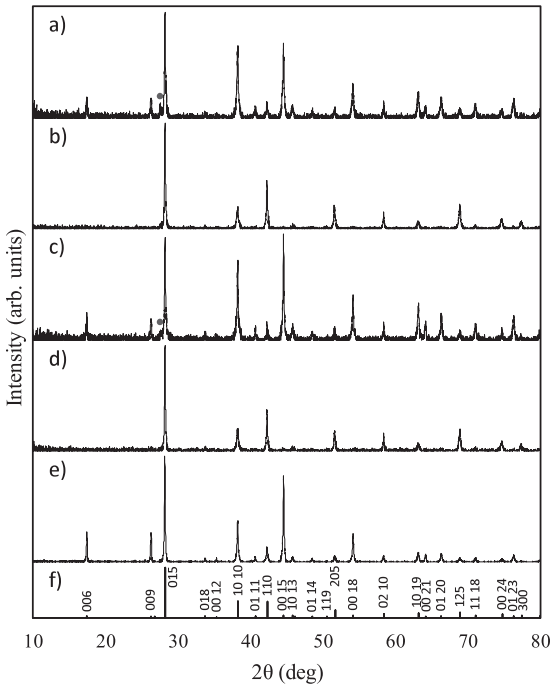

FIG. 6. XRD patterns (Cu Kα radiation) diffracted from the Sb_2Te_3 sintered sample prepared by (a) and (b) a current feed of 1.2 kA for 1 s, (c) and (d) the conventional ECAS process (773 K/3 min), and (e) original Sb_2Te_3 powder. (a) and (c) show the XRD patterns for the sample surface perpendicular to the compression direction during sintering. (b) and (d) show the XRD patterns obtained for the cross-section of the sample parallel to the compression direction. (f) is an XRD pattern taken from Anderson and Krause.[20] Unknown peaks are indicated by ●.

estimate the degree of grain alignment calculated from $(p - p_0)/(1 - p_0)$, where $p = \Sigma I(00l)/\Sigma I(hkl)$ for the 001-oriented sample, and $p_0 = p$ $(F = 0)$ for a randomly oriented sample,[18] the lower F value of 0.25 for the FS sample compared to the F value of 0.30 for the 3-min ECAS sample pointed to the lower degree of 00l-orientation in the FS sample. Therefore, the shortening of the sintering time might restrict the progress of the texture structure, which requires time to attain structural rearrangement by atomic diffusion in a solid. On the other hand, the presence of an impurity phase, such as an oxide, or a secondary phase or other crystal structure transformation was not detected. Furthermore, the difference in the peak position between the FS sample and that produced by conventional ECAS was negligibly small, such that the estimated lattice parameter for $a = 4.267$ Å, $c = 30.480$ Å for the FS sample was almost the same as that for $a = 4.266$ Å, $c = 30.484$ Å for the conventional ECAS sample. These XRD and SEM observation results indicated that the sintered Sb_2Te_3 sample could be obtained by the application of FS over some seconds, and would be of a similar level of quality to the sample prepared by the conventional ECAS method, but requiring several minutes to produce.

Finally, to determine the effect of FS on TE performance, the TE properties were evaluated. As shown in Fig. 7, all the FS samples produced with different levels of current feed exhibited almost the same S value, which was comparable to that of the sample prepared by conventional ECAS, but requiring some minutes to complete. Since the value of S depends on the electronic band structure and carrier density, its value and

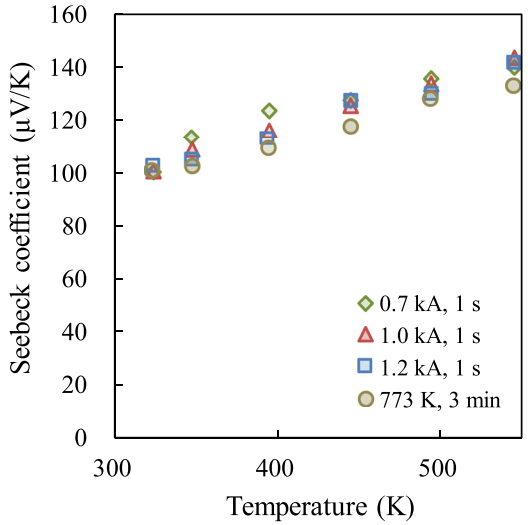

FIG. 7. Temperature dependence of Seebeck coefficient in sintered Sb_2Te_3 samples.

T-dependence are sensitive to the crystal lattice structure and chemical composition while being less affected by the microstructure. Therefore, this result for the value of S was consistent with the results of XRD analysis, as mentioned above.

On the other hand, regarding the transport properties, namely, σ and κ, which are easily affected by the microstructure, a difference in its magnitude was observed, as shown in Figs. 8 and 9. Although the T-dependence of σ, which is also sensitive to the electronic structure and carrier density in the same way as S, was identical, the FS sample produced with 1.2 kA exhibited a lower σ value compared to the ECAS sample, the production of which required some minutes. The lower density could be one of the reasons for the decrease in σ. In addition, the degree of grain alignment might also affect the value of σ because the Sb_2Te_3 possesses highly anisotropic transport properties such as $\sigma_{ab}/\sigma_c = 3$–4.[19] Since the value of σ was measured in the direction perpendicular to the compression axis during sintering, that is, along the

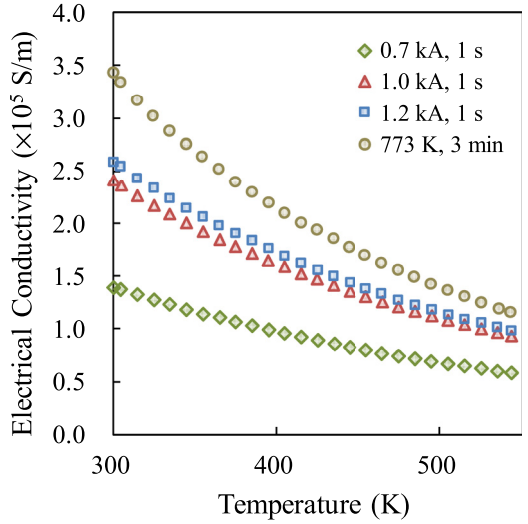

FIG. 8. Temperature dependence of electrical resistivity in sintered Sb_2Te_3 samples.

09 July 2025 02:46:38

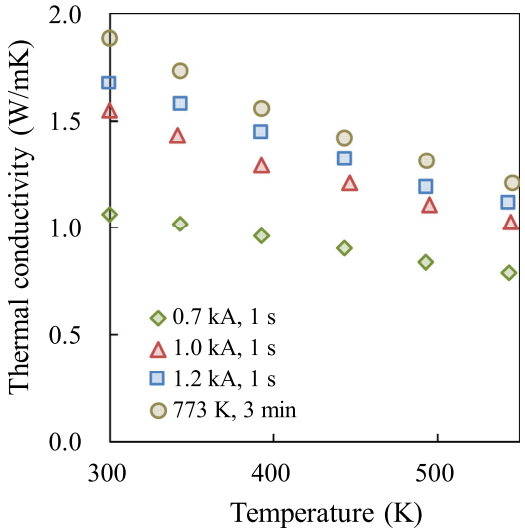

FIG. 9. Temperature dependence of thermal conductivity in sintered Sb_2Te_3 samples.

ab-plane preferred orientation, the lower degree of grain alignment could be a reason for the decrease in σ.

This difference in the microstructure also affected the value of κ, with the FS sample produced using 1.2 kA exhibiting a lower value of κ than the sample produced using ECAS, requiring some minutes. In the case of κ, however, since the measurement was made in the direction parallel to the compression axis, the lower degree of grain alignment could lead to an increase in the value of κ along the measuring direction because Sb_2Te_3 also has a highly anisotropic κ value of $\kappa_{ab}/\kappa_c \approx 4$. Therefore, the lower density of the FS sample could be the main reason for the decrease in the value of κ. Since σ and κ have opposite effects on the ZT value, the negative effect of the decrease in σ on the TE performance could be partially offset by the decrease in κ. This evaluation of the TE properties revealed that the FS sample exhibited small differences in the microstructure-sensitive transport properties of σ and κ while S remained identical.

IV. CONCLUSION

The flash sintering of thermoelectric materials was examined by FEM analysis and the practical evaluation of Sb_2Te_3 samples sintered with a current feed time of 1 s. The results of a FEM analysis suggested that uniform sample heating could be achieved by realizing a sufficiently high Joule-heating rate, relative to the thermal diffusion into the mold material. In addition, the possibility of a major reduction in the energy input required for sintering was indicated and, for the sintering of Sb_2Te_3, the ca. 80-Wh energy consumption of conventional ECAS (773 K/3 min) was actually reduced to 0.34 Wh for FS (1.2 kA/1 s). An evaluation of the FS samples confirmed that the crystallographic phase was unaffected by the significant acceleration in the heating rate while a slight reduction in the density and a degree of gain alignment was observed. The transport properties of σ and κ were slightly reduced while the value of S was identical. Since reductions in the values of σ and κ have opposite effects on the ZT value, the negative effect of FS on TE performance could be relatively small and limited although the ZT value could not be estimated accurately because of the difference in the measuring direction of σ and κ.

Since it could be assumed that the negative effect of FS on the microstructure was not an intrinsic problem related to FS but rather a result of the lower degree of process maturity in the present study, modification of the microstructure of the FS sample could be achieved by the further optimization of the sintering conditions and the powder preparation. Consequently, it seems reasonable to conclude that the sintered Sb_2Te_3 having a level of TE performance comparable to that produced by a conventional ECAS process could be fabricated by FS. This result demonstrates that a bulk TE material could be fabricated by ECAS in only a few seconds. Moreover, this result implies that other functional materials, which require precise control in terms of their chemical composition and crystallographic structure, could also be sintered by this method, although the specification of the power supply required for the FS apparatus should be modified according to the material conductivity. In addition, from a practical point of view, the large energy-conservation effect of FS appears to be extremely attractive, especially for the fabrication of the TE materials to be used for power generation aimed at energy recovery.

ACKNOWLEDGMENTS

This work was partly supported by the Adaptable and Seamless Technology Transfer Program through Target-driven R&D, A-STEP (No. AS2415009L), Japan Science and Technology Agency, JST.

[1]D. M. Rowe, *CRC Handbook of Thermoelectrics* (CRC press, Boca Raton, 1995).
[2]Y. Lan, A. J. Minnich, G. Chen, and Z. Ren, Adv. Funct. Mater. **20**, 357 (2010).
[3]K. Nielsch, J. Bachmann, J. Kimling, and H. Böttner, Adv. Energy Mater. **1**, 713–731 (2011).
[4]K. Biswas, J. He, I. D. Blum, C. I. Wu, T. P. Hogan, D. N. Seidman, V. P. Dravid, and M. G. Kanatzidis, Nature **489**, 414 (2012).
[5]S. Grasso, Y. Sakka, and G. Maizza, Sci. Technol. Adv. Mater. **10**, 053001 (2009).
[6]R. Orru, R. Licheri, A. M. Locci, A. Cincotti, and G. Cao, Mater. Sci. Eng., R **63**, 127 (2009).
[7]O. Guillon, J. Gonzalez-Julian, B. Dargatz, T. Kessel, G. Schierning, J. Rathel, and M. Herrmann, Adv. Eng. Mater. **16**, 830 (2014).
[8]W. S. Liu, B. P. Zhang, J. F. Li, H. L. Zhang, and L. D. Zhao, J. Appl. Phys. **102**, 103717 (2007).
[9]M. Scheele, N. Oeschler, K. Meier, A. Kornowski, C. Klinke, and H. Weller, Adv. Funct. Mater. **19**, 3476 (2009).
[10]B. Du, F. Gucci, H. Porwal, S. Grasso, A. Mahajan, and M. J. Reece, J. Mater. Chem. C **5**, 1514 (2017).
[11]M. Yu, S. Grasso, R. Mckinnon, T. Saunders, and M. J. Reece, Adv. Appl. Ceram. **116**, 24 (2017).
[12]M. Cologna, B. Rashkova, and R. Raj, J. Am. Ceram. Soc. **93**, 3556 (2010).
[13]S. K. Jha, K. Terauds, J. M. Lebrun, and R. Raj, J. Ceram. Soc. Jpn. **124**, 283 (2016).
[14]R. Chaim, G. Chevallier, A. Weibel, and C. Estournes, J. Mater. Sci. **53**, 3087 (2018).
[15]A. Karakuscu, M. Cologna, D. Yarotski, J. Won, J. S. C. Francis, R. Raj, and B. P. Uberuaga, J. Am. Ceram. Soc. **95**, 2531 (2012).
[16]J. A. Downs and V. M. Sglavo, J. Am. Ceram. Soc. **96**, 1342 (2013).
[17]D. Schwesig, G. Schierning, R. Theissmann, N. Stein, N. Petermann, H. Wiggers, R. Schmechel, and D. E. Wolf, Nanotechnology **22**, 135601 (2011).
[18]F. K. Lotgering, J. Inorg. Nucl. Chem. **9**, 113 (1959).
[19]M. Stordeur and W. Heiliger, Phys. Status Solidi B **78**, K103 (1976).
[20]T. L. Anderson and H. B. Krause, Acta Cryst. B **30**, 1307 (1974).

09 July 2025 02:46:38